Effects of nanoscale dispersion in the dielectric properties of poly(vinyl alcohol)-bentonite nanocomposites

María C. Hernández,[1,*] N. Suárez,[1] Luis A. Martínez,[1] José L. Feijoo,[2] Salvador Lo Mónaco,[3] and Norkys Salazar[4]
[1]*Departamento de Física, Universidad Simón Bolívar, Apartado 89000, Caracas 1080-A, Venezuela*
[2]*Departamento de Ciencias de los Materiales, Universidad Simón Bolívar, Apartado 89000, Caracas 1080-A, Venezuela*
[3]*Instituto de Ciencias de la Tierra, Facultad de Ciencias, Universidad Central de Venezuela, Apartado 47586, Caracas 1041-A, Venezuela*
[4]*Departamento de Química, Universidad Simón Bolívar, Apartado 89000, Caracas 1080-A, Venezuela*
(Received 16 November 2007; revised manuscript received 20 February 2008; published 2 May 2008)

We investigate the effects of clay proportion and nanoscale dispersion in the dielectric response of poly(vinyl alcohol)-bentonite nanocomposites. The dielectric study was performed using the thermally stimulated depolarization current technique, covering the temperature range of the secondary and high-temperature relaxation processes. Important changes in the secondary relaxations are observed at low clay contents in comparison with neat poly(vinyl alcohol) (PVA). The high-temperature processes show a complex peak, which is a combination of the glass-rubber transition and the space-charge relaxations. The analysis of these processes shows the existence of two segmental relaxations for the nanocomposites. Dielectric results were complemented by calorimetric experiments using differential scanning calorimetry. Morphologic characterization was performed by x-ray diffraction (XRD) and transmission electron microscopy (TEM). TEM and XRD results show a mixture of intercalated and exfoliated clay dispersion in a trend that promotes the exfoliated phase as the bentonite content diminishes. Dielectric and morphological results indicate the existence of polymer-clay interactions through the formation of hydrogen bounds and promoted by the exfoliated dispersion of the clay. These interactions affect not only the segmental dynamics, but also the secondary local dynamics of PVA.

DOI: 10.1103/PhysRevE.77.051801 PACS number(s): 82.35.Np, 77.84.Lf, 77.22.Ej, 64.70.Nd

I. INTRODUCTION

Polymer-inorganic nanocomposites have attracted great interest due to their improved properties in comparison with neat polymer or microscale composites like polymer-polymer blends or networks. There is a broad diversity in the inorganic nanofillers used depending on the intended application. This variety ranges from metal to insulators and includes spherical, cylindrical, and flake shapes [1–3]. Due to the nanoscale dispersion of the inorganic phase, very small filler content is enough to affect several properties on the polymer matrix. In polymer-clay nanocomposites the nanofiller is a smectite-type layer silicate with an interlayer spacing between individual sheets of about 1 nm thick. These individual silicate sheets with lateral dimension of about 1 μm are piled up parallel to each other and coupled with weak electromagnetic forces of dipolar or van der Waals origin. The interlayer coupling in natural smectites usually involves inorganic cations (such as Li^+, Na^+, K^+, Ca^{2+}, and Mg^{2+}) attached to the negatively charged silicate surface [4]. Depending on the experimental technique used, as well as on the compatibility between the clay and the polymer matrix, three basic types of clay dispersion are possible: (a) a microphase-separated compound with tactoids formation, (b) a clay-polymer intercalation with an increase in the interlayer spacing, and (c) an exfoliated morphology with individual silicate sheets dispersed within the polymer matrix [4]. In order to provide detailed microstructural information about clay dispersion in polymer nanocomposites, a combination of x-ray diffraction (XRD) and transmission electron microscopy (TEM) is needed [5,6]. Different experimental techniques have been developed to produce intercalated and exfoliated polymer-clay morphologies. Typically the first step involves the improvement of clay-polymer compatibility, usually through organic modification of the clay via a cation-exchange process in which the inorganic cation is replaced with a higher-molecular-weight organic cation [7]. The next step for nanocomposite preparation is related to the clay blending in the polymer through monomer polymerization, melt blending, or solvent casting procedures [5–8]. In water-soluble polymers such as poly(ethylene oxide) or poly(vinyl alcohol), it is possible to obtain a good clay dispersion without the organic modification of the clay through the solvent casting method in water because of the hydrophilic character of most natural smectites [9]. Earlier studies of polymer-clay nanocomposites have focused on preparation, structural information, and thermal or mechanical improvements of the polymer matrix [4]. Over the last years attention has centered on understanding how the polymer-clay interaction and morphology correlate with the dynamic behavior of the polymer matrix at different scales. Because of the high surface-to-volume ratio of clays, it is expected that even for low filler content, a highly dispersed configuration allows a high fraction of polymer-clay interphase, and depending on the intermolecular interactions, a modification of the polymer molecular mobility appears [10]. For intercalated morphologies the modification in chain dynamics is associated with nanoconfinement caused by dimensional restrictions of nanometric scale [11,12]. As a consequence of the cooperative nature of the glass-rubber transition, usually the study of macromolecules dynamics in polymer-clay nanocomposites is re-

*mahernan@usb.ve

stricted to the segmental mobility associated with the glass transition temperature of the polymer. Several studies about molecular dynamics in these systems have been performed including mechanical [5,7,12], dielectric [10,11,13] and thermal analysis [14]. For materials with dielectrically active segments, the use of techniques such as dielectric spectroscopy or thermally stimulated depolarization current (TSDC) are of great interest to explore intra- and intermolecular interactions in polymer nanocomposites. Due to its low equivalent frequency, the TSDC technique is particularly effective resolving polymer dynamics at different scales ranging from segmental and high-temperature cooperative relaxations [15–17] to local secondary relaxations [18–20]. Besides, a wide variety of systems such as copolymers [18], polymer blends [19], liquid crystals [21], and polymer nanocomposites [13,22,23] have been recently studied with the TSDC technique. The high resolution and sensitivity obtained with the TSDC technique makes it important for the exploration of polymer dynamics in nanocomposites [24]. The effects on molecular mobility around the glass-rubber transition when a nanoscale clay dispersion is present are far from being elucidated. Several studies report an increase of the glass transition temperature—i.e., a slowing down of the segmental relaxation—in intercalated and exfoliated morphologies [14] and silica nanocomposites [25]. This behavior has been explained as a consequence of the restricted molecular mobility of attached chains on the clay surface. In contrast, similar morphologies show a speedup (decreasing on T_g) of the glass-rubber relaxation with the addition of silicate clay [10,12] which is ascribed to local free-volume changes or dimensional restrictions. In complex systems with different molecular dynamics it is possible to observe two different segmental relaxations. In polymer-nanoparticle composites the appearance of two separate glass-rubber transitions has been reported in a variety of materials. Usually one of the glass transitions is associated with the bulk polymer matrix while the other is related to polymer-inorganic interactions in the interphase zone around the nanofiller. The new glass-rubber transition is observed both above [14,23] and below [11] the bulk polymer segmental relaxation in clay and silica nanocomposites. These behaviors are explained as the appearance of a new zone near the polymer-clay interphase in which the polymer-filler interactions produce dramatic changes in polymer dynamics. It is expected that strong polymer-clay interactions also affect the noncooperative subglassy relaxations. Detailed studies of the effect of nanoscale inorganic dispersion on local dynamics are rarely reported [22]. A comprehensive understanding of the local and cooperative dynamic behavior near the polymer-clay interphase is incomplete and requires further investigation. In the present work a study of the polymer-clay interactions and morphology effects in the polymer dynamics at different scales is presented for a series of poly(vinyl alcohol)-bentonite (PVA-be) nanocomposites. We use a high-resolving-power and high-sensitivity dielectric technique (TSDC), which allows us to resolve the molecular mobility on different scales: from local secondary relaxations to cooperative segmental and interphase processes. The dynamic characterization of the amorphous phase was complemented by and correlated with polymer-clay effects on the crystalline phase through calorimetric results [differential scanning calorimetry (DSC)]. In addition, morphology studies with XRD and TEM characterization were also performed. These complementary studies allow a more complete picture of the effects of the polymer-clay interaction and morphology on the dynamical behavior of the amorphous and crystalline polymer phases.

II. EXPERIMENT

A. Materials

The clay used is a natural montmorillonite (bentonite) obtained from Minersis (Santiago, Chile), under the trade name of W-140P. The poly(vinyl alcohol) (PVA, $[-CH_2CH(OH)]_n-$) is a product of Fluka with a degree of hydrolysis of 98% and a $M_w=47{,}000$ g mol^{-1}.

B. Sample preparation

The PVA-be nanocomposites were prepared by a solvent casting procedure. The bentonite was suspended in distilled water at room temperature and sonicated for 30 min in an ultrasonic bath; the PVA is diluted in distilled water and stirred for the same time in a magnetic hot plate stir at a temperature of 85 °C. Both solutions are then mixed in a common beaker, stirred for additional 60 min at 85 °C, and poured onto a glass plate. The nanocomposite film formed was left to dry out at room temperature for several days. The film preparation for the neat PVA is identical, except for the absence of the clay blending step.The PVA-be nanocomposites studied have a bentonite content of 0, 1, 2, and 5 wt % in PVA.

C. X-ray diffraction

For the x-ray diffraction (XRD) analysis, a Bruker AXS model D8 was used, covering in the diffractograms the 2θ range from 1.5 to 13, with a Cu Kα radiation of $\lambda = 1.5406$ Å.

D. Transmission electron microscopy

A JEN-1220 was used for TEM studies; samples were prepared using pieces of film from each composition that were cast in epoxy used as a matrix. Films were microtomed into 100–200-nm slices and placed on a copper grid and imaged with an accelerating voltage of 100 kV.

E. Thermally stimulated depolarization current

TSDC experiments are performed in a high-vacuum cell and measuring system designed in our laboratory. The sample is disk shaped, 18 mm in diameter and 200 mm thick, located inside the TSDC cell between two parallel-plate capacitors, with sapphire disks of 20 mm diameter placed between the sample and the plates. In order to prevent moisture effects, all samples were carefully dried in a high-vacuum environment at room temperature for several days. In the polarization protocol a voltage $V_p=400$ V is applied at the polarization temperature T_p during a time t_p (typically 3 min), long enough to reach the equilibrium polarization at

this temperature. In the course of polarization a pure nitrogen atmosphere is used. Once the time t_p takes place, the sample is quenched and the equilibrium polarization is frozen in; at the final temperature of 80 K, the voltage is turned off and the depolarization protocol begins. In this protocol, the cell is filled with helium gas, the sample is connected to an electrometer (Cary Vibrating Reed model 401 M), and the depolarization current is automatically recorded as the temperature rises at a constant rate of $b=6$ K min^{-1}. The polarization conditions are chosen to properly separate secondary sub-T_g relaxations from the glass-rubber transition and higher-temperature relaxations.

F. TSDC analysis

The low-temperature secondary relaxations are studied by the direct signal analysis (DSA) method [26]. This method is a numerical deconvolution of a global TSDC spectrum in N elementary Debye processes, each of them described by the Arrhenius equation for the relaxation time $\tau(T)$. The basic idea is to decompose a complex spectrum in N elementary relaxations equally spaced in an energy interval whose combination best fits the whole experimental TSDC data, without any assumption about the distribution of the relaxation times. This method has been successfully used in studies of hydrogen-bonded effects in moisture nylon-6 [27], triblock copolymers [18] and blends of policarbonate-poly(ϵ-caprolactone) at different extents of miscibility [19]. The high-temperature TSDC spectra may show a complex behavior with important modifications in profile and position depending on the polymer interactions and nanoheterogeneities. Within this zone it is expected to observe the glass-rubber transition and the space-charge relaxation. To characterize the glass transition relaxation peak, the dipolar contribution is described by the Williams-Landel-Ferry (WLF) zeroth-order approximation for the temperature dependence of $\tau(T)$ [28]. According to this model the dipolar contribution to the current density can be expressed as

$$J_{\alpha i}(T) = J_{0i}\frac{\exp[\beta_i(T-T_{gi})]}{\exp[\eta_i(T-T_{gi})/T]+1}, \tag{1}$$

where β_i, η_i, J_{0i}, and T_{gi} are constants that characterize the shape and position of the glass transition relaxation. The charge redistribution relaxation peak, the conduction part of the current density, can be described with the expression

$$J_Q(T) = Q_0 f(T)\left(\alpha + \frac{1}{T}\right)\exp[-f(T)], \tag{2}$$

with $f(T)=\frac{T}{b\tau_0}\exp[\alpha(T-T_g)]$ where b is the heating rate, α and τ_0 are constants related to the WLF approximation for $\tau(T)$, and Q_0 is proportional to the intensity of the charge peak. This model has been successfully used to study the effects of structural relaxation on the glass transition temperature and charge redistribution peak for tyrosine-derived polycarbonates [15] and polyarylates [29].

G. Differential scanning calorimetry

In order to determine the differences in thermal properties of the polymer and nanocomposites samples, studies of DSC were employed using a Perkin-Elmer DSC-7; sample weights of $5.0-7.0\pm0.1$ mg were used. The samples were sealed in aluminum pans under a nitrogen atmosphere of high purity. The rank of temperatures studied went from 273 to 523 K and heated at the scanning rate of 20 K min^{-1}; at least two samples of the same composition were used for each run. The temperature was controlled with a precision not less than ±0.1 K over the whole measured temperature interval. T_g measurements were determined using the midpoint inflection method. First scans were used in order to obtain T_g, T_m, T_c, and ΔH_f. The heat of fusion, ΔH_f, is determined by the area under the melting peaks by integration of melting exotherms and is directly proportional to the degree of crystallinity (X_c), which can be calculated by

$$X_c = \frac{\Delta H_f}{(1-w_b)\Delta H^*}\times 100, \tag{3}$$

where w_b is the weight fraction of the filler in the nanocomposite and ΔH^* is the heat of fusion for an infinitely large crystal. In the case of PVA [30], ΔH^* was reported to be 138.6 J g^{-1}.

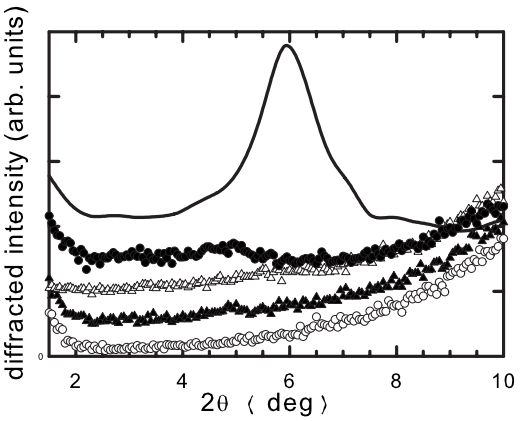

FIG. 1. XRD spectra of bentonite, PVA, and PVA-be nanocomposites: (solid line) bentonite, (●) PVA-be 5%, (△) PVA-be 2%, (▲) PVA-be 1%, and (◯) PVA.

III. RESULTS AND DISCUSSION

A. XRD and TEM results

Figure 1 presents the XRD curves for all nanocomposites. The main diffraction peak of bentonite around $2\theta=6$ corresponds to the basal interlayer distance with $d_{(100)\text{be}}=14.7$ Å. For the PVA-be 5%, a broad and small peak can be observed at $4.5<2\theta<5$, with a mean interlayer distance of $d_{(100)\text{be}5}=18.7$ Å. This shift to lower angles of the basal spacing from natural bentonite to the PVA-be 5% is consistent with partial polymer intercalation into the clay galleries at this composition. This diffraction peak is absent for the low-clay-content samples PVA-be 2% and PVA-be 1%, indicating an important exfoliated morphology at these compositions.

In order to complement the XRD results, TEM micrographs of all samples were made and are presented in Fig. 2 as (a), (b), and (c) for PVA-be 5%, PVA-be 2%, and PVA-be 1%, respectively.

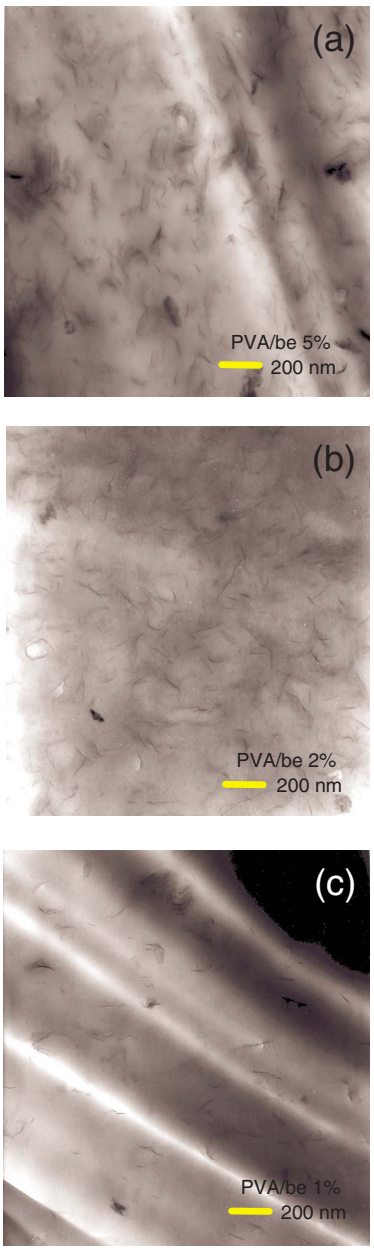

FIG. 2. (Color online) TEM micrographs: (a) PVA-be 5%, (b) PVA-be 2%, and (c) PVA-be 1%.

TEM results show an important fraction of exfoliated clay dispersed in PVA. XRD results, together with TEM characterization, indicate that at the PVA-be 5% composition, partially intercalated arrays are formed, and when the clay content decreases, the exfoliated extent is improved as the individual sheets of clay are more dispersed within the polymer matrix.

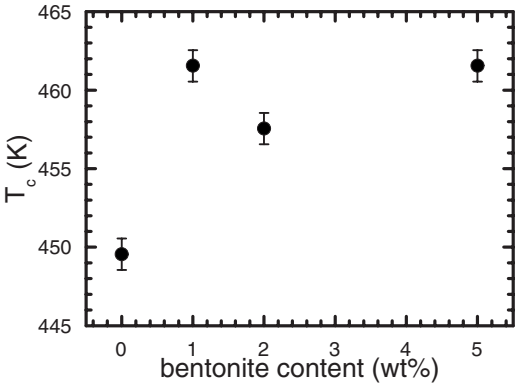

FIG. 3. Crystallization temperature as a function of bentonite content.

B. DSC results

The effect of the content of bentonite in the crystallization behavior of PVA was studied. The relevant thermal transitions and enthalpies are listed in Table I.

Figure 3 shows representative data concerning the influence of bentonite content on the crystallization temperature of PVA. As can be seen, the T_c of PVA increases with the presence of bentonite. This result indicates the nucleation effect of the surface of the bentonite, which may be driven by the strong specific interactions between the PVA and the silicate. Specifically, the vinyl alcohols of the PVA form hydrogen bonds with the surface oxygen of silicates [31]. This behavior is not dependent on the final morphology of the nanocomposite—i.e., exfoliated and/or intercalated. The influence on the degree of crystallization of PVA due to the presence of bentonite is shown in Fig. 4. The increase in the amount of clay reduces the extent of the bulk crystallization of PVA. There is a reduction of almost 20% in crystallinity as can be seen in the graph. In spite of being a good nucleating agent, the increase in the content of clay reduces the extent of the crystallization, as shown in Fig. 3. This result may be explained on the basis of different interactions of the surface of the clay with the polymer, independently if the interactions occur with exfoliated surfaces or intercalated surfaces. In particular, the main interaction would correspond to the formation of hydrogen bonds between the PVA hydroxyl groups and water adsorbed on bentonite surface. This contributes to the reduction of the crystallinity of PVA due to the reduction of the interchain hydrogen bonds responsible

TABLE I. Calorimetric results of PVA and PVA-be nanocomposites.

Sample	$T_g \pm 1$ (K)	$T_m \pm 1$ (K)	$T_c \pm 1$ (K)	ΔH_f (J/g)	X_c
poly(vinyl alcohol)	320	492	450	76.5	0.552
PVA-be 1%	301	493	462	65.0	0.474
PVA-be 2%	303	496	458	53.2	0.392
PVA-be 5%	297	493	462	49.3	0.374

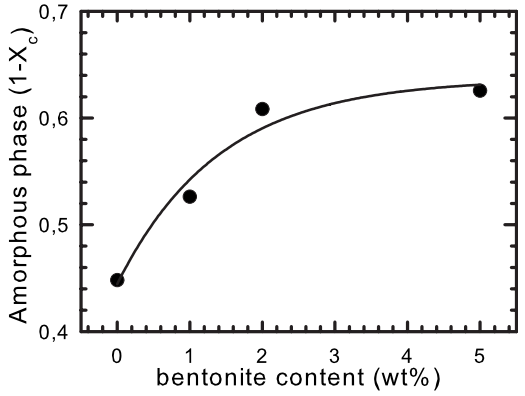

FIG. 4. Amorphous phase fraction as a function of bentonite content. Solid line is drawn to guide the eye.

for the crystallization of PVA. Studies of the crystalline phase of similar PVA-MMT nanocomposites have been done by Strawhecker and Manias [9,32].

These investigations demonstrate the nucleating nature of bentonite, driven by the strong specific interactions between the PVA and the silicate. These authors affirm that the crystals grown on the MMT surface are associated with hydrogen bonds between PVA groups and the silicate oxygen atoms [32]. The decrease in the heat of fusion as the clay content increases has been reported in PVA-MON blends [33] and is associated with the reduction of PVA crystallinity by well-dispersed montmorillonite. The study of polymer crystallization in clay nanocomposites and its comparison with the inorganic phase morphology is a subject far from been elucidated. In particular, for PVA nanocomposites the influence of clay dispersion and hydrogen-bonding interactions introduce additional complications to the analysis.

C. TSDC results

Figure 5 shows (as symbols) the TSDC spectra between 80 and 230 K, corresponding to the secondary relaxations of neat PVA and the PVA-be nanocomposites studied.

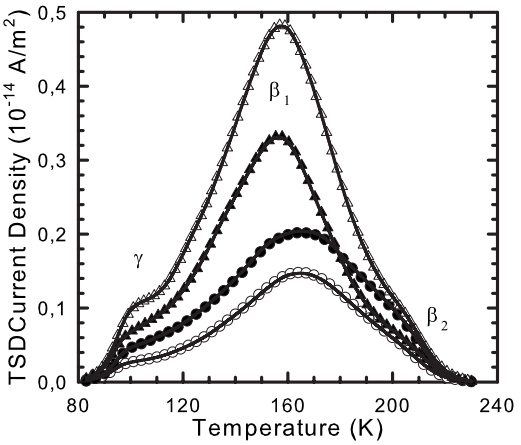

FIG. 5. Low-temperature TSDC spectra of PVA and PVA-be nanocomposites: (◯) PVA, (▲) PVA-be 1%, (△) PVA-be 2%, and (●) PVA-be 5%. Solid lines correspond to the fitting results.

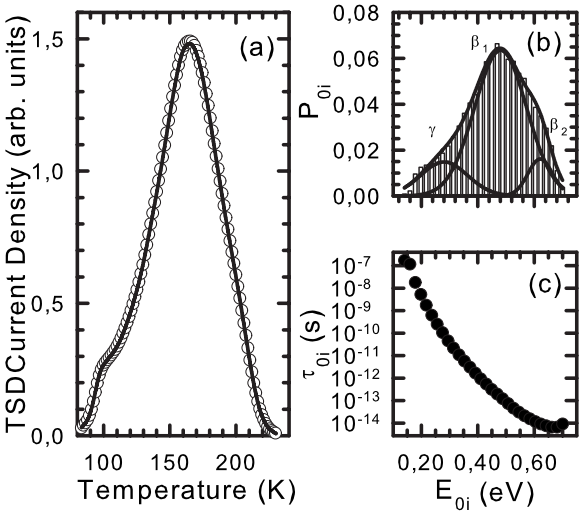

FIG. 6. DSA results for the PVA secondary relaxations: (a) (◯) experimental data and (solid line) fit. (b) Energy histogram with the contribution of each elementary Debye process to the total polarization. (c) Preexponential factor dependence with the activation energy.

The spectra were polarized at T_p=220 K with a normalization of 1 MV m^{-1}. In this figure it is possible to appreciate broad multicomponent relaxations with three main complex modes (γ, β_1, and β_2, around 100, 160, and 200 K, respectively) whose relative contribution modifies substantially the spectra profile for each sample. The weaker spectrum corresponds to the PVA homopolymer, while the stronger spectra correspond to the lower-clay-content samples (PVA-be 1% and PVA-be 2%). These latter samples also exhibit a low-temperature shift of the β_1 mode. The differences observed indicate important changes in the reorientable dipolar species responsible for the processes that originate local molecular dynamics as the clay dispersion is improved. In order to quantify the local relaxations effects of clay dispersion, a numerical decomposition of these spectra is made and the relaxation time distribution is obtained [26]. This is performed assuming the existence of 30 elementary Debye processes (enough to guarantee an adequate convergence), with a temperature dependence of the relaxation time described by the Arrhenius equation. The parameters obtained for the fitting procedure are the preexponential factor τ_{0i}, the activation energy E_{0i}, and the elementary contribution to the total polarization, P_{0i}. The result of the relaxation time distribution for a typical analysis is presented in Fig. 6 for neat PVA.

In Fig. 6(a) the experimental data (open circles) and numerical fit (solid line) are presented. The excellent fit observed corresponds to a sum of squared residuals of $\chi^2 \sim 10^{-10}$. Similar fitting results are obtained for the rest of the samples and plotted as solid lines in Fig. 5. The polarization corresponding to each elementary Debye peak as a function of its activation energy is shown in Fig. 6(b). In Fig. 6(c) is presented the dependence of the preexponential factor with the activation energy of each elementary process. The energy histogram was fitted to three main relaxations, assuming Gaussian profiles, labeled as γ, β_1, and β_2 and shown in Fig.

6(b) as solid lines. Secondary relaxations in PVA are related to noncooperative rotation of OH side groups and local twisting motions about the main chain (crankshaft motion) [34]. The presence of hydroxyl groups originates strong effects on the polymer properties due to the formation of inter- and intramolecular hydrogen bonds between OH groups or between OH and absorbed moisture; the formation of H bonds between neighboring OH groups can be used to explain the existence of a high crystalline phase in this polymer without any specific stereoregularity [34]. Investigations of the low-temperature relaxations of PVA consist of both mechanical [34–37] and dielectric [34,35,38,39] studies. The mechanical results include the appearance of two distributed processes, named as γ and β modes [34,35], or one very broad secondary relaxation labeled as β [36,37]. Dielectric results in the frequency domain only show a single broad relaxation identified as β relaxation [34,35,38,39]. As a consequence of its low equivalent frequency, the TSDC technique allows one to resolve three distributed processes γ, β_1, and β_2, with mean activation energies of $E_{a\gamma} = (27 \pm 8)$ kJ/mol [(0.28 ± 0.08) eV], $E_{a\beta 1} = (46 \pm 9)$ kJ/mol [(0.48 ± 0.09) eV], and $E_{a\beta 2} = (60 \pm 4)$ kJ/mol [(0.62 ± 0.04) eV] for pure PVA. Here the Gaussian distribution width for each process is used as an overestimated uncertainty for comparison with previous results. The activation energies reported for the β mode in frequency dielectric experiments performed in PVA, including dry samples at different crystallinities, are the following: $E_{a\beta} = (55 \pm 3)$ kJ/mol [34], $E_{a\beta} = 52$ kJ/mol [35], and $E_{a\beta} = 59$ kJ/mol [38]. Our TSDC results reveal that the β mode is composed of two overlapping processes β_1 and β_2, which could not be resolved at the frequency domain. The activation energies reported for the β mode would be an average of the β_1 and β_2 modes clearly resolved by TSDC. In fact, an attempt to resolve numerically this overlapping is made by De La Rosa *et al.* [38], finding two processes with activation energies of 40 and 66 kJ/mol. On the other hand, to our knowledge, there are no previous mechanical or dielectric experimental results reporting secondary γ relaxation for PVA. This mode, due to its low activation energy, could be associated with localized rotations of small lateral groups (hydroxyl groups) or absorbed molecules. Numerical simulations of PVA dynamics using atomistic models [40] give an estimation of $E_{a\gamma} = (11 \pm 4)$ kJ/mol for local reorientation movements of hydroxyl groups, which should be used as the lower limit for the activation energy of this relaxation. Some comparison has been done between vinyl polymers and polysaccharides, in order to elucidate the common origin of local conformational changes of polar side groups [37,38]. Dielectric results on dextran and cellulose [41] report for the hydroxyl groups rotation in dextran, an activation energy of $E_{a\gamma dex} = (32 \pm 9)$ kJ/mol, and a numerical deconvolution of secondary dielectric results in cellulose gives the same activation energy $E_{a\gamma cell} = 32$ kJ/mol for the hydroxyl group rotation. These activation energies are in good agreement with our results for the γ relaxation in PVA. The former discussion allows us to assume a common origin for the noncooperative conformational changes in side OH for dextran, cellulose, and poly(vinyl alcohol), with similar activation energy. To quantify the effect of clay dispersion on the secondary relaxations of PVA, a comparison of the mean activation energy [Fig. 7(a)] and polarization [Fig. 7(b)] for each component as a function of clay content is made.

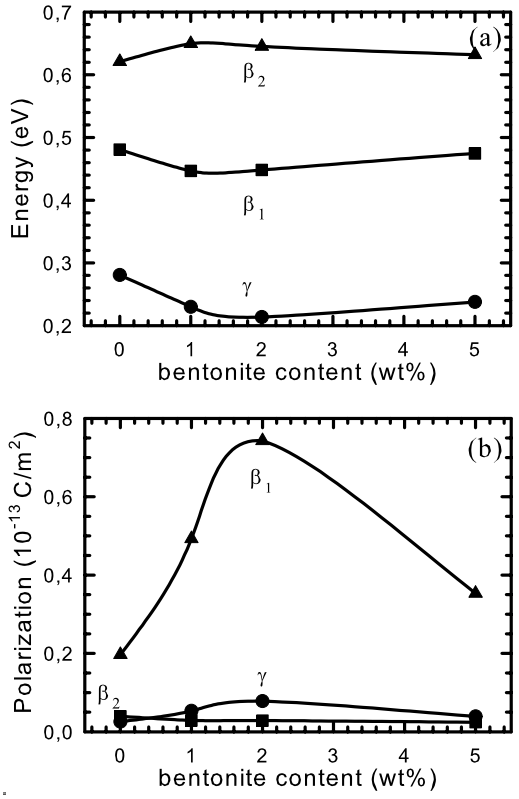

FIG. 7. DSA analysis for the PVA and PVA-be nanocomposites: (a) mean activation energy and (b) contribution to the polarization, as a function of bentonite content. Solid line is drawn to guide the eye.

As contrasted to neat PVA, the activation energy of the γ mode for all the nanocomposites shifts to lower energies with a nearly constant value of (0.23 ± 0.01) eV. The activation energy of the β_1 and β_2 modes for PVA-be 5% is almost the same as that obtained for equivalent modes in neat PVA. For the PVA-be 1% and PVA-be 2% samples a shift to lower energies of the β_1 mode and a slight shift to higher energies for the β_2 mode are observed in comparison to neat PVA. The relative contribution of each mode to the polarization of the secondary relaxation is presented in Fig. 7(b). The trend observed indicates an important promotion of the main process, the β_1 mode, with the addition of dispersed clay. This effect is improved at the lower bentonite content (PVA-be 1% and PVA-be 2%) where the clay dispersion is enhanced. The same trend is observed for the γ mode, with a factor of approximately 3 between the relative polarization of neat PVA and PVA-be 2% samples. The β_2-mode contribution to polarization does not show a noticeable variation with bentonite content. Contrasting the results presented in Figs. 7(a) and 7(b), it can be affirmed that the β_2 mode is almost insensitive to the addition of clay in PVA. As this is the higher-energy mode, the β_2 process could be a partially activated relaxation related to the Johary-Goldstein T_g precursor. A different behavior is observed by the γ and β_1 modes in which a plasticization effect—i.e., a reduction of

the activation energy and improvement of chain mobility—is produced at the lower clay content. This behavior could be associated with water firmly attached to specific polar sites, probably by forming hydrogen bonds [42]. Due to the hydrophilic character of the natural bentonite used, the presence of water attached at the clay surface is expected. As the samples studied are all carefully dried before their characterization, it is reasonable to state that any moisture effects on polymer dynamics come from this firmly bound clay-attached water. In PVA the hydrogen bonds are the dominant interaction responsible for both structure and molecular dynamics. As a consequence of these bonding interactions, water is capable to destroy inter- and intrachain hydroxyl bounds, affecting crystalline regions in PVA and acting as a plasticizer by inducing the rise in the free-volume size in the amorphous phase [43]. A possible interpretation of the results obtained indicates that at the PVA-bentonite interphase, clay-attached water induces a rupture in the inter- and intrachain hydrogen-bonded hydroxyl groups, forming a new H bond with one of the OH groups. The remained free hydroxyl group is now able to contribute to the polarization with local OH conformational motions (origin of the γ mode) or with a more cooperative relaxation associated with local motions of chain segments (β_1 mode). The small lowering of the activation energy observed in both relaxations suggests a slight increase in the free volume around the polymer-clay interphase, indicating a disruption of polymer chain packing around the inorganic phase; a similar behavior has been reported in polymer-fumed silica nanocomposites [44]. In our PVA nanocomposites the effect over the γ and β_1 relaxations is enhanced at the lower clay content, when the clay dispersion is mostly in the exfoliated state and a larger area of the clay is exposed to the polymer matrix. Dielectric studies of secondary relaxations in polymer nanocomposites are scarcely reported. In PMMA+SiO_2 nanocomposites [22], the observed effects on the side-chain relaxation of PMMA are associated with hydrogen-bonded interactions between silica and ester carbonyls. In contrast, in PVA nanocomposites [35], no effects on the γ and β relaxations have been reported in both mechanical and dielectric characterizations. Therefore to the best of our knowledge, the presence of this effect is being discussed for the first time in this work. The TSDC characterization of the high-temperature relaxations, between 200 and 310 K, is presented in Fig. 8 (as symbols) for PVA-be nanocomposites and neat PVA.

The polarization temperature was T_p=296 K, and the spectra were normalized to 1 MV m^{-1}. Similar TSDC experiments performed at a polarization temperature of 345 K demonstrate the absence of relaxation processes between 300 and 345 K for all samples measured. The relaxations observed in this figure show a complex behavior with important modifications in profile and peak positions for all samples studied. Within this temperature range, it is expected to observe the dielectric manifestation of the glass-rubber transition (segmental relaxation), as well as the contribution of the space-charge redistribution peak due to the presence of blocking electrodes [15,29]. In order to properly quantify the contribution of each relaxation process to the TSDC spectra, a combination of Eqs. (1) and (2) is used, by means of a standard nonlinear fitting procedure. To obtain reliable results, the existence of two segmental relaxations must be considered. Within these assumptions the high-temperature TSDC relaxations can be expressed as

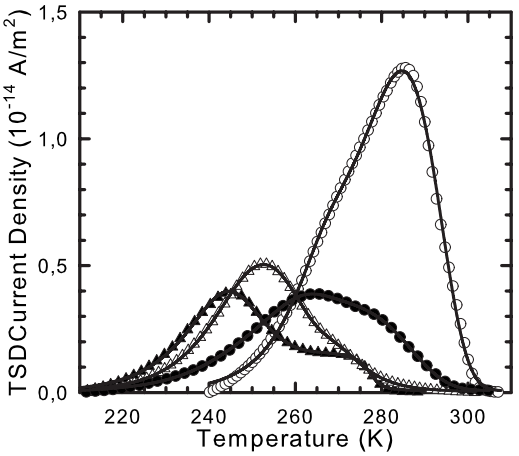

FIG. 8. High-temperature TSDC spectra of PVA and PVA-be nanocomposites: (◯) PVA, (▲) PVA-be 1%, (△) PVA-be 2%, and (●) PVA-be 5%. Solid lines correspond to the fitting results.

$$J(T) = J_{\alpha 1}(T) + J_{\alpha 2}(T) + J_Q(T), \tag{4}$$

the high-temperature segmental relaxations, and J_Q is the conduction contribution to the depolarization current. The solid lines in Fig. 8 show the fitting results for all samples studied using Eq. (4). It is important to note that for the neat PVA spectrum, the numerical analysis applying Eq. (4) produces only one segmental relaxation; i.e., the contribution of $J_{\alpha 1}$ to the TSDC spectra is neglected in this sample. Figure 9 presents a typical deconvolution of the high-temperature TSDC spectrum for the PVA-be 5% nanocomposite; in this figure, the solid line represents the low-temperature segmental relaxation $J_{\alpha 1}$, and the high-temperature segmental relaxation ($J_{\alpha 2}$) is represented as a dotted curve.

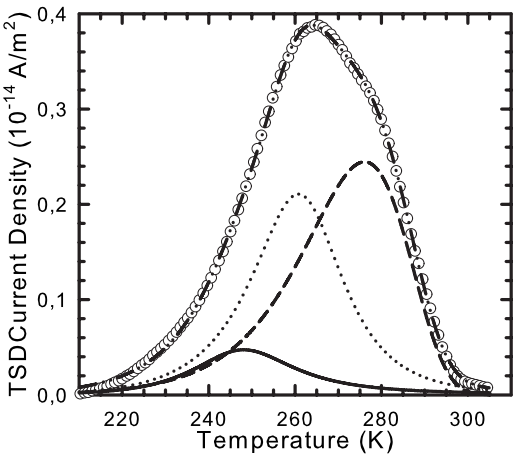

FIG. 9. Deconvolution of the high-temperature TSDC spectrum for the PVA-be 5% nanocomposite: (◯) experimental data, (solid line) $J_{\alpha 1}(T)$, (dotted line) $J_{\alpha 2}(T)$, (dashed line) $J_Q(T)$, and (dot-dashed line) total.

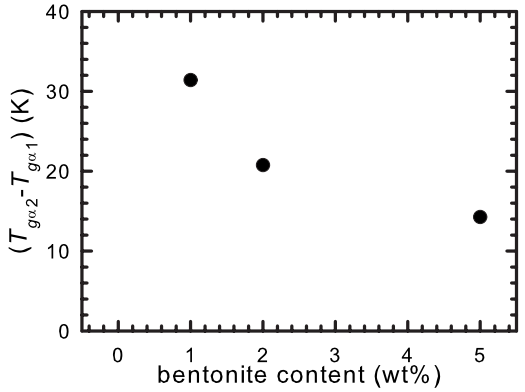

FIG. 10. Split of the segmental relaxations as a function of bentonite content.

This analysis shows the existence of two segmental dynamics as a consequence of clay dispersion. Therefore, there are two glass-rubber transition temperatures associated with this complex segmental relaxation process. Figure 10 shows the split of the two glass transition temperatures (plotted as $T_{g\alpha 2}-T_{g\alpha 1}$) as a function of clay content.

The trend observed in Fig. 10 demonstrates the existence of two clearly distinguished molecular dynamics at the scale of the segmental relaxations, which separate in temperature as the clay dispersion is improved (i.e., as the extent of exfoliated bentonite increases). Figure 11 presents the glass transition temperatures obtained dielectrically ($T_{g\alpha 1}$ and $T_{g\alpha 2}$) and its comparison with DSC results as a function of the amorphous phase.

In this figure the solid triangles ($T_{g\,\mathrm{mean}}$) are obtained averaging the two glass transitions observed dielectrically. The $T_{g\,\mathrm{mean}}$ in Fig. 11 shows that both calorimetric and dielectric measurements present the same trend as a function of the amorphous phase. The possibility of distinguishing two segmental dynamics with the TSDC results (observed as one mean T_g by DSC) is related to the high resolving power of this dielectric technique, associated with its low equivalent frequency. Similar results are reported in miscible blends where nanoheterogeneities produce two different segmental

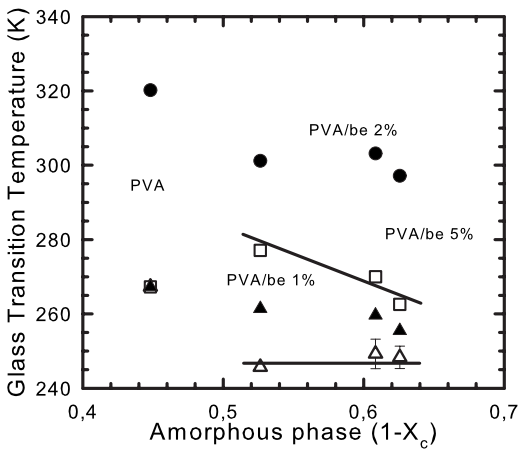

FIG. 11. Glass transition temperatures as a function of the amorphous phase: (△) $T_{g\alpha 1}$, (□) $T_{g\alpha 2}$, (▲) $T_{g\,\mathrm{mean}}$, and (●) $T_{g\,\mathrm{DSC}}$. Straight lines are drawn to guide the eye.

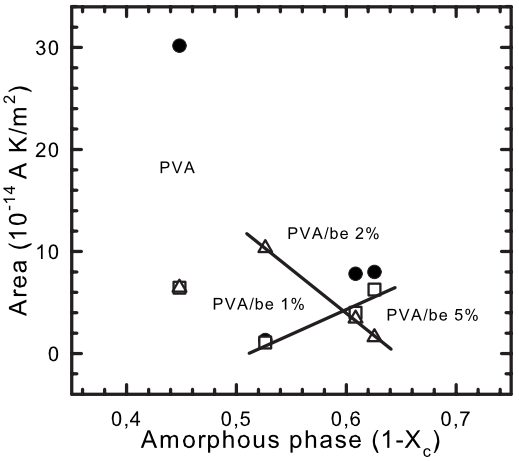

FIG. 12. High-temperature TSDC area of each relaxation process as a function of the amorphous phase: (●) $J_Q(T)$, (△) $T_{g\alpha 1}$, and (□) $T_{g\alpha 2}$. Straight lines are drawn to guide the eye.

dynamics observed dielectrically by the TSDC technique [17,45], but detected as one glass-rubber transition by DSC. In polymer nanocomposites, the observation of different segmental dynamics, depending on the resolution of the experimental technique, is discussed in poly(methyl acrylate) with fluoromica [46] comparing spin-label electron spin resonance and DSC. As observed in Fig. 11 all the calorimetric glass transitions are above the dielectric $T_{g\,\mathrm{mean}}$ in about 40 K. The differences in heating rates of both techniques (20 K/min for DSC and 6 K/min for TSDC) might explain in part this variation [47]. In addition, as the dried process for both techniques is different, a lower content of residual water molecules is expected in samples used for the calorimetric studies. In PVA water contents below 5% could plasticize in more than 30 K, the glass transition temperature [43]. In order to complement the analysis of the high-temperature relaxations, Fig. 12 presents the TSDC area of each relaxation process as a function of the amorphous phase.

For the segmental relaxations two different trends are observed: the area of the low-temperature relaxation α_1 (open triangles) increases as the amorphous phase diminishes (with the improvement of bentonite dispersion); by the other side, the high-temperature relaxation α_2 (open squares) diminishes its $J(T)$ area with the decrease of the amorphous phase. The charge redistribution relaxation area (solid circles) shows an important reduction with the addition of the inorganic phase. This behavior for the charge relaxation is consistent with changes in the amorphous-crystalline interphase with the presence of the inorganic phase. For dipolar processes, the areas under a $J(T)$ curve are representative of the number of dipoles in the amorphous phase whose reorientation contributes to the total polarization. Comparing Figs. 11 and 12, the existence of two distinct dynamics in the amorphous zone at the scale of the cooperative molecular motions associated with the segmental relaxation is clear. The low-temperature segmental relaxation α_1 (open triangles in Figs. 11 and 12) shows a shift to low temperature of T_g (around 20 K in comparison to neat PVA), and an increase of the number of reorientable molecular chains as the bentonite dispersion improves (i.e., as the fraction of polymer-clay interfacial region

increases). These results are consistent with the presence of important polymer-clay interactions responsible for this new segmental dynamics at the amorphous zone surrounding individual clay palettes. The enhancement in molecular mobility associated with the shift to lower temperatures of the $T_{g\alpha 1}$ suggests that polymer-clay interactions in this zone induce an increase in the free volume. This explanation is consistent with the results obtained on the γ and β_1 modes for the secondary relaxation and interpreted as the results of hydrogen-bonded interactions between hydroxyl groups and firmly bonded clay-attached water. In our results, the same mechanism responsible for the plasticization of the local modes may be used to explain the results obtained for the low-temperature segmental relaxation. As the scale of molecular movements is larger in segmental modes, the effects of such hydrogen-bonded assisted polymer-clay interactions are more evident at the high-temperature relaxations. Similar results on exfoliated poly(propylene-graft-maleic anhydride) organophilic clays with local free-volume enhancement have been reported [10]. The high-temperature segmental relaxation (α_2) is presented in Figs. 11 and 12 as open squares and shows a rise in the glass transition temperature among a drop in the number of reorientable molecular chains as crystallinity increases. Assuming that this relaxation is related with the bulk amorphous phase, the areas for all nanocomposites fall bellow the linear dependence between peak area and amorphous content [18] when a comparison with neat PVA is made. These results are consistent with a strong hindering effect on the cooperative motions for this relaxation as a consequence of crystal-amorphous interactions [48]. The presence of a rigid amorphous phase for the nanocomposites must be a consequence of constraints imposed by the crystalline phase and the clay morphology as the intercalated dispersion increases.

IV. CONCLUSIONS

The effects on the amorphous and crystalline phases due to clay dispersion and polymer-clay interactions have been studied in PVA-bentonite nanocomposites using a whole variety of experimental techniques such as DSC, XRD, TEM, and TSDC. Morphologic results reveal an important presence of exfoliated morphology for all compositions with an improvement in clay dispersion as bentonite content diminishes. Even though in the crystalline phase the clay acts as a nucleating agent, the overall PVA crystallization diminishes with increases of the clay content. This behavior is the result of two types of hydrogen-bonded polymer-clay interactions in competition. For the amorphous phase of PVA, the TSDC results reveal important effects on polymer dynamics with the addition of bentonite. For the low-temperature secondary relaxations, better clay dispersion promotes local modes with a plasticization effect. This behavior is explained as the result of polymer-clay hydrogen-bonded interactions mediated by firmly bonded clay-attached water. TSDC results at the high-temperature relaxations reveal the existence of two segmental dynamics for the nanocomposites: a low-temperature segmental relaxation associated with the fraction of polymer-clay interfacial region which is influenced by hydrogen-bound interactions with firmly bounded clay-attached water and a high-temperature segmental relaxation driven by the crystalline phase and clay morphology.

ACKNOWLEDGMENTS

Financial support from the Fondo Nacional de Ciencia Imnovación y Tecnología (FONACIT) through the Project No. G-2005000449 and from the DID (Universidad Simón Bolívar) are gratefully acknowledged.

[1] A. M. Testa, S. Foglia, L. Suber, D. Fiorani, Ll. Casas, A. Roig, E. Molis, J. M. Grenèche, and J. Tejada, J. Appl. Phys. **90**, 1534 (2001).
[2] Z. H. Mbhele, M. G. Salemane, C. G. C. E. va Sittert, J. M. Nedeljkovgic, V. Djokovic, and A. S. Luyt, Chem. Mater. **15**, 5019 (2003).
[3] D. Daoukaki, G. Barut, R. Pelster, G. Nimtz, A. Kyritsis, and P. Pissis, Phys. Rev. B **58**, 5336 (1998).
[4] T. J. Pinnavaia, *Polymer-Clay Nanocomposites*, Wiley Series in Polymer Science (Wiley, New York, 2001).
[5] L. Y. Jiang and K. H. Wei, J. Appl. Phys. **92**, 6219 (2002).
[6] V. Krikorian and D. Pochan, Chem. Mater. **15**, 4317 (2003).
[7] P. Maiti, K. Yamada, M. Okamoto, K. Ueda, and K. Okamoto, Chem. Mater. **14**, 4654 (2002).
[8] X. Huang and W. J. Brittain, Macromolecules **34**, 3255 (2001).
[9] K. E. Strawhecker and E. Manias, Chem. Mater. **12**, 2943 (2000).
[10] M. Bohning, H. Goering, A. Fritz, K. W. Brzezinka, G. Turky, A. Schonhals, and B. Schartel, Macromolecules **38**, 2764 (2005).
[11] K. A. Page and K. Adachi, Polymer **47**, 6406 (2006).
[12] Y. Rao and J. M. Pochan, Macromolecules **40**, 290 (2007).
[13] R. A. Vaia, B. B. Sauer, O. K. Tse, and E. P. Giannelis, J. Polym. Sci., Part B: Polym. Phys. **35**, 59 (1997).
[14] H. Lu and S. Nutt, Macromolecules **36**, 4010 (2003).
[15] M. C. Hernández and N. Suárez, Polymer **45**, 8491 (2004).
[16] N. Suárez, M. Puma, M. C. Hernández, and J. Walter, J. Appl. Phys. **99**, 1135241 (2006).
[17] E. Leroy, A. Alegría, and J. Colmenero, Macromolecules **35**, 5587 (2002).
[18] E. Laredo, M. C. Hernández, A. Bello, M. Grimau, A. J. Müller, and V. Balsamo, Phys. Rev. E **65**, 021807 (2002).
[19] M. C. Hernández, E. Laredo, A. Bello, P. Carrizales, L. Marcano, V. Balsamo, M. Grimau, and A. J. Müller, Macromolecules **35**, 7301 (2002).
[20] I. M. Kalogeras, E. R. Neagu, and A. Vassilikou-Dova, Macromolecules **37**, 1042 (2004).
[21] N. Nikonorova, T. Borisova, E. Barmatov, P. Pissis, and R. Diaz-Calleja, Macromolecules **36**, 5784 (2003).
[22] I. M. Kalogeras and A. Vassilikou-Dova, J. Phys. Chem. B **105**, 7651 (2001).

[23] D. Fragiadakis, P. Pissis, and L. Bokobza, Polymer **46**, 6001 (2005).
[24] V. M. Gunko *et al.*, Adv. Colloid Interface Sci. **131**, 1 (2007).
[25] D. Fragiadakis, P. Pissis, and L. Bokobza, J. Non-Cryst. Solids **352**, 4969 (2006).
[26] M. Aldana, E. Laredo, A. Bello, and N. Suárez, J. Polym. Sci., Part B: Polym. Phys. **32**, 2197 (1994).
[27] E. Laredo and M. C. Hernández, J. Polym. Sci., Part B: Polym. Phys. **35**, 2879 (1997).
[28] M. Puma, Polym. Adv. Technol. **8**, 39 (1997).
[29] M. Puma and N. Suarez, J. Appl. Polym. Sci. **69**, 283 (1998).
[30] N. A. Peppas and P. J. Hansen, J. Appl. Polym. Sci. **27**, 4787 (1982).
[31] J. C. Grunlan, A. Grigorian, C. B. Hamilton, and A. R. Mehrabi, J. Appl. Polym. Sci. **93**, 1102 (2004).
[32] K. E. Strawhecker and E. Manias, Macromolecules **34**, 8475 (2001).
[33] N. Ogata, S. Kawakage, and T. Ogihara, J. Appl. Polym. Sci. **66**, 573 (1997).
[34] N. G. McCrum, B. E. Read, and G. Williams, *Anelastic and Dielectric Effects in Polymer Solids* (Dover, New York, 1991), p. 327.
[35] I. Cendoya, D. López, A. Alegría, and C. Mijangos, J. Polym. Sci., Part B: Polym. Phys. **39**, 1968 (2001).
[36] E. El Shafee and H. F. Naguib, Polymer **44**, 1647 (2003).
[37] A. De La Rosa, L. Heux, and J. Y. Cavaillé, Polymer **41**, 7547 (2000).
[38] A. De La Rosa, L. Heux, and J. Y. Cavaillé, Polymer **42**, 5371 (2001).
[39] B. Schartel, J. Wendling, and J. H. Wendorff, Macromolecules **29**, 1521 (1996).
[40] A. De La Rosa, L. Heux, J. Y. Cavaillé, and K. Mazeau, Polymer **43**, 5665 (2002).
[41] H. Montes and J. Y. Cavaillé, Polymer **40**, 2649 (1999).
[42] J. Vanderschueren and A. Linkens, Macromolecules **11**, 1228 (1978).
[43] R. M. Hodge, T. J. Bastow, G. H. Edward, G. P. Simon, and A. J. Hill, Macromolecules **29**, 8137 (1996).
[44] T. C. Merkel, B. D. Freeman, R. J. Spontak, Z. He, I. Pinnau, P. Meakin, and A. J. Hill, Science **296**, 519 (2002).
[45] H. Shimizu, S. Horiuchi, and T. Kitano, Macromolecules **32**, 537 (1999).
[46] Y. Miwa, A. R. Drews, and S. Schlick, Macromolecules **39**, 3304 (2006).
[47] K. Noris-Suárez, J. Lira-Olivares, A. M. Ferreira, J. L. Feijoo, N. Suárez, M. C. Hernández, and E. Barrios, Biomacromolecules **8**, 941 (2007).
[48] M. Arnoult, E. Dargent, and J. F. Mano, Polymer **48**, 1012 (2007).